

International Journal of Image and Graphics  
© World Scientific Publishing Company

## ACTIVE DEFORMABLE MODELS USING DENSITY ESTIMATION

Wael Abd-Elmageed

*Computer Vision Laboratory  
Institute for Advanced Computer Studies  
University of Maryland  
College Park, MD 20742  
wamageed@ieee.org*

Christopher E. Smith

*Department of Electrical and Computer Engineering,  
University of New Mexico,  
Albuquerque, New Mexico 87131, USA  
chsmith@ece.unm.edu*

Received (17 September 2002)

Revised (13 March 2003)

Accepted (31 March 2003)

This paper introduces a new approach to active deformable models. The paper starts with a brief review of the relevant approaches. We then use the Expectation Maximization and Parzen Window techniques to develop a more robust formulation for pressure snakes. The generic nature of the proposed model allows it to perform well on complex colored images. We show, by several examples, the enhanced performance of the snake under the new formulation, compared to the performance of other known snake formulations.

*Keywords:* Active Contour Models; Pressure Snakes; Expectation Maximization; Mixture of Gaussians; Parzen Window.

### 1. Introduction

Active deformable models, more commonly known as snakes, have received considerable attention for more than a decade since their introduction. These models attract much of this attention because of certain characteristics. For instance, they can segment objects with a lower computational cost than equivalent, complete methods. They also give a piecewise linear description of the occluding contour of the object with no additional processing. Finally, they can track objects from frame-to-frame in a video sequence without specifically solving the correspondence problem.

Unfortunately, snakes are not without their problems. The traditional snake formulation, introduced by Kass et al. <sup>7</sup>, requires a solution to a system of partial differential equations. Since solving systems of partial differential equations can-

not be performed efficiently, finite difference methods are used and applied in a serial update fashion that performs only localized solutions. Additionally, the classic snake uses image gradient as a driving function, leading to a transform of the original image via discrete convolution. This typically is an edge detection step that approximates the image gradient. Convolution adds computational overhead while throwing away possibly relevant image data (appearance, color, texture, etc.). The snakes also tended to collapse in weak image gradients, leading to the incorporation of balloon forces designed to prevent this collapse. All of these issues make snakes hard to implement, tune, and use.

To address some of these problems, Ivins and Porrill<sup>5</sup> introduced a form of snakes known as statistical pressure snakes. These models use image data directly and are based upon techniques of statistical region growing. Pressure snakes could use virtually any statistical pixel measure, including color, texture, or spatial frequency. Objects must be of constant pixel value for this method to succeed.

A logical question to ask is; whether other techniques beyond the simple statistical methods can be employed to allow the snakes to segment and track complex objects in imagery with complex backgrounds. Certainly techniques from pattern recognition theory can be borrowed and applied to the pressure snakes, but, will this necessarily lead to enhanced performance on targets that cannot be segmented by the original methods of Ivins and Porrill<sup>5</sup>?

In this paper, we present work that extends upon the original Ivins and Porrill snakes by incorporating more sophisticated pattern matching and modeling techniques. These techniques allow the snake to perform well under non-laboratory conditions and across a variety of object and background colorations. Throughout the paper, we will interchangeably use color and graylevel, because in gray scale images, the intensity is the only measure of the color of the object.

The remainder of the paper begins with a discussion of the relevant prior work on snakes in Section 2. In Section 3, a method for automatically estimating pressure snake parameters is presented. In Section 4, we introduce a new generic pressure model to overcome the drawbacks of Ivins and Porrill's pressure model. Section 5 presents some experimental results obtained by applying the proposed algorithms. The paper is concluded in Section 6.

## 2. Literature Review

### 2.1. *Classic Snakes*

The classical snake was first presented by Kass et al.<sup>7</sup>. This snake is placed onto a potential field derived from the image and allowed to change shape and position, minimizing the energy along the length of the curve. The energy functional is defined as:

$$E = \int_0^1 E_{\text{Snake}}(S(u))du, \quad (1)$$

where  $S(u)$  represents the snake. In the case of closed contours,  $S(0) = S(1)$ . The snake's energy,  $E_{Snake}$ , at a certain point,  $u$ , is the weighted sum of the internal energy, the image energy or potential (edges, corners, or dark spots on the image) and external energy (e.g., employing user-selected points as attractors). The external energy term could be used to reshape the contour, biasing it toward some local shape. Eq. 2 describes the total energy of the snake.

$$E = \int_0^1 (E_{\text{Internal}}(S(u)) + E_{\text{External}}(S(u)) + E_{\text{Image}}(S(u))) du \quad (2)$$

The internal energy, given Eq. 3, of the contour consists of a tension component, represented by a first-order derivative, and a stiffness/curvature component, represented by a second-order derivative,

$$E_{\text{Internal}}(S(u)) = \frac{\alpha}{2} \left| \frac{\partial S(u)}{\partial u} \right|^2 du + \frac{\beta}{2} \left| \frac{\partial^2 S(u)}{\partial u^2} \right|^2 du, \quad (3)$$

where  $\alpha$  and  $\beta$  are weights.

The image potential  $P(S(u))$ , representing the internal energy, is defined as the image edges and is used to approximate gravity for the virtual weights energy. It is most common for image energy to be estimated as the result of edge detection. For example, the image energy can be computed as

$$E_{\text{Image}} = -(G_\sigma \otimes \nabla^2 I)^2, \quad (4)$$

where the Laplacian,  $\nabla^2 I$ , of the image is convolved with a Gaussian kernel,  $G_\sigma$ . The result is squared to account for positive and negative edges, and the negative of this magnitude is used in order to attract the contour to a local minima.

The total snake energy, dropping the external energy term, is then represented by Eq. 5

$$E = \frac{\alpha}{2} \oint \left| \frac{\partial S(u)}{\partial u} \right|^2 du + \frac{\beta}{2} \oint \left| \frac{\partial^2 S(u)}{\partial u^2} \right|^2 du + \oint P(S(u)) du \quad (5)$$

The image energy term is calculated from the image edges in the neighborhood around each control point of the snake. The energy is minimized when a control point is located on the steepest part of the gradient. Most snakes in use today are based upon Kass et al. snakes and they retain the use of edge detection as a measure of image gradient.

## 2.2. Statistical Pressure Snakes

One of the first problems associated with the traditional formulations of Kass et al. <sup>7</sup> is that in the absence of image gradient, these models tended to collapse. Therefore, a strong gradient field is preferred to drive the snake. On the other hand, in stronger gradient fields, the placement of the snake has to be carefully

4 *W. Abd-Almageed and C. E. Smith*

chosen, so that the snake does not collapse to a local minimum away from the object. In fact, a segment of the snake must cross the gradient associated with the region of interest. A question now arises. If we have the strong edges needed to drive the snake, why do we have to use snakes? In other words, why do we not use a simpler edge linking technique, to segment the object of interest?

To overcome these limitations, balloon snakes were developed by Choen and Note<sup>8</sup> where they added a new internal pressure term to force the model to expand, as described by Eq. 6.

$$E = \frac{\alpha}{2} \oint \left| \frac{\partial S(u)}{\partial u} \right|^2 du + \frac{\beta}{2} \oint \left| \frac{\partial^2 S(u)}{\partial u^2} \right|^2 du + \frac{\rho}{2} \oint \frac{\partial S(u)}{\partial u} \times S(u) du + \oint P(S(u)) du \quad (6)$$

The new term is the third term in Eq. 6. Unfortunately, the new pressure term introduces new problems with the model. For instance, the initial placement of the snake had to be within the target (a constraint that still remains in many models). Also, in weak gradient fields, the balloon snakes tend to explode rather than collapse.

The proposed solution by Ronfard<sup>9</sup> was a dynamic pressure model. Ronfard's method incorporated a term that, by computing the similarity of pixel values around the snake control points, created a force that would push the points toward region boundaries. Scale spaces were used to capture region boundaries that lie outside the local neighborhood.

Ivins and Porrill<sup>5</sup> paralleled this line of research by proposing several forms of dynamic pressure models. These models overcome the need to change scales by having a region well defined not just locally but across the entire image. The pressure models are based upon low order statistics and utilize a seed region of the image to identify positive versus negative pressure regions. In other words, image regions that are statistically similar to the seed region yield positive pressure while image regions that are some number of standard deviations away from the seed yield negative pressure. When a portion of the contour is in a positive region, it will expand the contour. When a portion of the contour is in a negative region, it will contract. It follows that the minimum energy of the contour lies on the pressure boundary between the positive and negative regions. This work can be viewed as the application of statistical segmentation to the snake image force.

The pressure force used by Ivins and Porrill<sup>5</sup> is as follows. A seed region is selected from within the target. The mean  $\mu$  and standard deviation  $\sigma$  of the intensity for the seed region are computed. The image force is then given by:

$$\vec{F}(S(u)) = \left( 1 - \frac{|I(S(u)) - \mu|}{k\sigma} \right) \left( \frac{\partial S(u)}{\partial u} \right)^\perp, \quad (7)$$

where  $S$  is the curve and  $k$  is a user specified parameter, that signifies the Bayesian decision boundary. The  $\perp$  indicates that the image force is perpendicularly applied

to the tangent of the contour. This model is a linear pressure model where the image force increases linearly away from a zero when the image intensity is  $k$  standard deviations to either side of the mean.

Many possible pressure forces can be used with these snakes, including terms based upon color, texture, spatial frequency, etc.; however they still calculate pressure in a similar manner to the original mean and standard deviation pressure model. This model is much too simple to allow the snakes to be used outside of the laboratory except in special cases where the imagery favors such modeling. One application of these types of snakes to real imagery is a synthetic aperture radar (SAR) automatic target recognition system that has been incorporated as a toolbox in the Khoros imaging system. In this application, SAR imagery corresponds well to the simple mean-standard deviation model.

### 3. Automatic Estimation of Pressure Snake Parameters

Pressure snakes alleviate the need for detecting strong edges. However, three drawbacks can be observed in the new pressure model of Eq. (7). First, the parameter  $k$  must be accurately selected to obtain good snake performance. Fig. 1 illustrates the importance of selecting  $k$ . The mean and standard deviation of the object distribution are 20 and 20, respectively. If  $k$  is set wrongly to 2 and the image intensity at the contour is  $x = 61$ , Eq. (7) will produce negative pressure although the intensity is more similar to the object than to the background, which has a very narrow distribution with a mean of 200. Second,  $\mu$  and  $\sigma$  are low order statistics that are sufficient only to describe simple colored objects. Finally, the model accounts only for the color of the object of interest. It does not account for the color of the background.

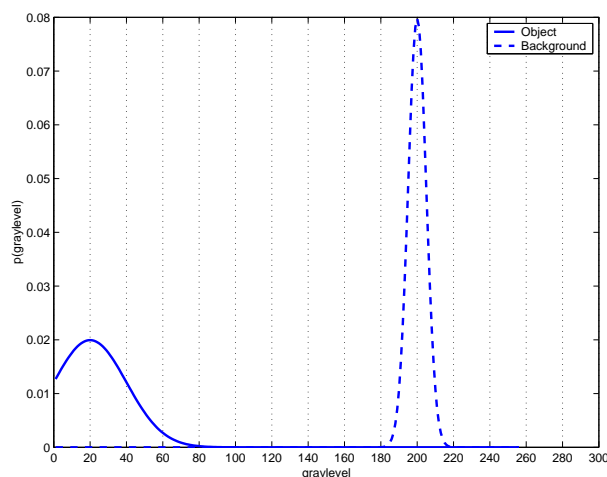


Fig. 1.  $k$  must be selected accurately

6 *W. Abd-Almageed and C. E. Smith*

To automatically estimate the values of  $\mu$ ,  $\sigma$  and  $k$ , we add one more assumption to the pressure model defined by Eq. (7). We assume that the background is simple colored and can be represented by low order statistics, as was assumed for the object color. From the two assumptions, the probability  $p(x|I)$  that a gray level  $x$  belongs to the image  $I$  can be represented as a mixture of two Gaussian distributions (one for the object and one for the background) as follows:

$$p(x|I) = \sum_{j=1}^{m=2} \pi_j p(x|j) \quad (8)$$

where

$$p(x|j) = \frac{1}{\sqrt{2\pi}\sigma_j} \exp\left(-\frac{(x - \mu_j)^2}{2\sigma_j^2}\right), \quad (9)$$

and  $\pi_j$  is weight of component  $j$  in the mixture and  $\sum_{i=1}^m \pi_i = 1$ .

The six values of  $\mu_j$ ,  $\sigma_j$  and  $\pi_j$  can be estimated by applying the Expectation Maximization (EM) <sup>10</sup> algorithm to the set of training pixels  $\mathbf{X} = \{x_i : i = 1, 2, \dots, N\}$  of size  $N$ , as follows.

Let  $\Gamma^{i-1}$  denote the sum of posterior probabilities of  $\mathbf{X}$  evaluated using the model obtained at iteration  $i - 1$ , and is defined as:

$$\Gamma_j^{i-1} = \sum_{\forall x \in \mathbf{X}} P^{i-1}(j|x), \quad (10)$$

where the posterior probabilities  $P(j|x)$  are given by Eq. (11) from Bayes theorem <sup>11</sup>. Update Eqs. (12), (13) and (14) are then applied to  $\mathbf{X}$  in the following order.

$$P(j|x) = \frac{\pi_j p(x|j)}{p(x|I)}, \quad (11)$$

$$\mu_j^i = \frac{\sum_{\forall x \in \mathbf{X}} x P(j|x)}{\Gamma_j^{i-1}}, \quad (12)$$

$$\pi_j^i = \frac{\Gamma_j^{i-1}}{N} \quad \text{and} \quad (13)$$

$$\sigma_j^i = \frac{\sum_{\forall x \in \mathbf{X}} P^{i-1}(j|x)(x - \mu_j^i)^2}{\Gamma_j^{(i-1)}}. \quad (14)$$

Applying the update equations repeatedly monotonically increases the likelihood, and hence converging to a local maximum. This suggests that the resulting values will strongly depend on the initial values (i.e.  $\mu_j^0$ ,  $\sigma_j^0$  and  $\pi_j^0$ .) Thus, to initialize component means,  $\mu_j^0$ , we run the K-means <sup>12</sup> clustering algorithm for a small number of iterations. The standard deviations,  $\sigma_j^0$ , are initialized by clustering the  $N$  pixels using the Euclidian distance to  $\mu_j$ , and computing the standard deviation of the pixels in each of the two clusters. The initial weights,  $\pi_j^0$ , are initialized to  $1/2$ .

The optimal decision boundary  $x^*$  between the object and background can then be computed by solving the equation

$$\frac{\pi_1}{\sqrt{2\pi}\sigma_1} \exp\left(\frac{-(x^* - \mu_1)^2}{2\sigma_1^2}\right) = \frac{\pi_2}{\sqrt{2\pi}\sigma_2} \exp\left(\frac{-(x^* - \mu_2)^2}{2\sigma_2^2}\right), \quad (15)$$

which yields

$$x^* = \frac{-b \pm \sqrt{b^2 - 4ac}}{2a}, \quad (16)$$

where

$$a = \frac{1}{2}(\sigma_2^2 - \sigma_1^2), \quad (17)$$

$$b = \mu_2\sigma_1^2 - \mu_1\sigma_2^2, \quad \text{and} \quad (18)$$

$$c = \frac{1}{2}(\mu_1^2\sigma_2^2 - \mu_2^2\sigma_1^2) - \sigma_1^2\sigma_2^2(\log\frac{\pi_1}{\pi_2} + \log\frac{\sigma_2}{\sigma_1}). \quad (19)$$

Eq. (16) yields two solutions. We pick the solution that lies between  $\mu_1$  and  $\mu_2$ . From Ivins and Porrill assumption in <sup>5</sup>, we know which mode is the object mode (i.e. we know  $\mu_O$  and  $\sigma_O$ .) Thus, an optimal value for  $k$  can be computed as

$$k = \frac{|\mu_{\text{Object}} - x^*|}{\sigma_{\text{Object}}}. \quad (20)$$

#### 4. A More Generic Pressure Model

In the previous section, we introduced a statistically optimal method for estimating the parameters of pressure snakes introduced by Ivins and Porrill <sup>5</sup>. This method solves the problem of manually tuning the system parameters. However, the more important problems of the color complexity of both object and background, discussed in Section 3, still exist.

The motivation for developing a more robust and generic pressure model is clear. The most common case is complex colored objects and/or background. Thus, low order statistics are not enough for representing either the object or the background. A more generic model will be of the form

$$\vec{F}(S(u)) = (p(\mathbf{x}|O) - p(\mathbf{x}|B)) \left( \frac{\partial S(u)}{\partial u} \right)^\perp, \quad (21)$$

where  $O$  and  $B$  denote the object and background, respectively. The term  $(p(\mathbf{x}|O) - p(\mathbf{x}|B))$  represents the magnitude of the force to be applied perpendicular to the tangent of the contour. To even make this model more generic,  $\mathbf{x}$  now denotes any feature vector of length  $|\mathbf{x}| \geq 1$ .

There are three main advantages of using this model. First, the model does not make any assumptions on the color complexity of the object. Second, the background is taken into consideration. Finally, the model is defined for any higher dimensional feature vector, not only the gray level.

The problem is now reduced to that of estimating the PDFs of both object and background. In the next two sections we employ two well-known PDF estimation techniques. A brief comparison between the two techniques is later given in Section 6.

#### 4.1. Parametric Estimation of the PDFs

To estimate  $p(\mathbf{x}|O)$  and  $p(\mathbf{x}|B)$ , we use an approach similar to the one used to estimate the model parameters in Section 3. Each of  $p(\mathbf{x}|O)$  and  $p(\mathbf{x}|B)$  is modeled as a mixture of Gaussians as follows:

$$p(\mathbf{x}|k) = \sum_{j=1}^{m_k} \pi_j p(\mathbf{x}|j) \quad ; \quad k = O \quad \text{or} \quad B \quad (22)$$

where

$$p(\mathbf{x}|j) = \frac{1}{\sqrt{2\pi}|\Sigma_j|^{\frac{1}{2}}} \exp\left(-\frac{1}{2}(\mathbf{x} - \mu_j)^T \Sigma_j^{-1} (\mathbf{x} - \mu_j)\right). \quad (23)$$

The EM algorithm is then used twice to estimate the models' parameters, one for the object model parameters and the other for the background model parameters. The update Eqs. (12) and (13) are used with the exception that the quantities  $\mu_j$  and  $\mathbf{x}$  are vectors, and Eq. (14) is replaced by

$$\Sigma_j^i = \frac{\sum_{\forall \mathbf{x} \in \mathbf{X}} P^{i-1}(j|\mathbf{x})(\mathbf{x} - \mu_j^i)(\mathbf{x} - \mu_j^i)^T}{\Gamma_j^{i-1}}, \quad (24)$$

for estimating the covariance matrix,  $\Sigma_j^i$ . All parameters are initialized using the same procedure as discussed in Section 3. The values of  $m_O$  and  $m_B$  are defined manually in our experiments. However, any algorithm, such as <sup>13</sup>, can be used to provide an automatic estimate for them.

#### 4.2. Non-parametric Estimation of the PDFs

Parzen <sup>14</sup> provides a non-parametric method for estimating the probability density function from a set of training data  $\mathbf{X} = \{\mathbf{x}_i : i = 1, \dots, N\}$ . The PDF is estimated by

$$p(\mathbf{x}) = \frac{1}{hN} \sum_{i=0}^N \Phi(|\mathbf{x} - \mathbf{x}_i|), \quad (25)$$

where  $h$  is the width of the histogram bin and  $\Phi(\mathbf{x})$  is called the kernel function. Several kernel functions could be used in the estimation process. In our experiments, we use the Gaussian kernel function described by Eq. (26).

$$\Phi(\mathbf{x}) = \frac{1}{\sqrt{2\pi}} \exp\left(-\frac{1}{2}\mathbf{x}^T \mathbf{x}\right). \quad (26)$$

Figs. (2), (3) and (4) show a multi-colored image, the histogram of its intensity values and the PDF estimated using Parzen Windows, respectively. We use a histogram bin width of,  $h = 1$ .



Fig. 2. Complex Colored Image

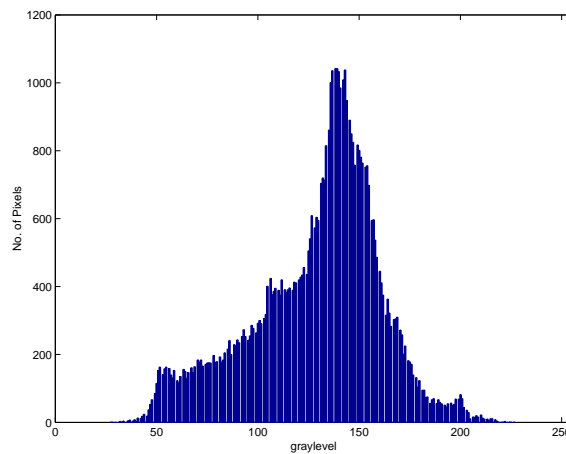


Fig. 3. Histogram of the Image of Fig. (2)

## 5. Experimental Results

In all of the following experiments, we apply the proposed model to gray scale images. However, the model can also be applied to images in any other color space, such as RGB, HSI or Lab. In such case,  $\mathbf{x}$  will represent a feature vector.

Fig. (5) is an example that verifies the validity of the approach of Section 3. The Figure shows a simple colored object (black rectangle) on a simple colored background. The histogram of the gray level values of Fig. (5) and the estimated PDFs are shown in Figs. (6) and (7), respectively. The estimated  $k$ , using the approach in Section 3, coincides with the Bayesian decision boundary.

Fig. (8) shows a complex colored background (pendulum base) that is used in a pendulum tracking application. Figs. (9) and (10) represent the histogram and the estimated PDF, using a mixture of two Gaussian components, for Fig. (8). The

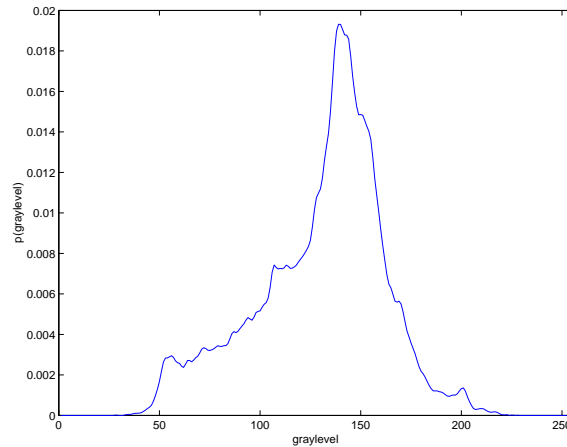


Fig. 4. PDF of the Image of Fig. (2)

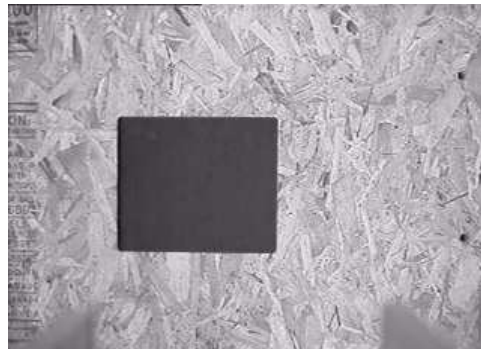


Fig. 5. Simple Colored Object and Background

segmentation result of the pendulum using the pressure model of Ivins and Porrill is shown in Fig. (11), with the model parameters  $\mu$ ,  $\sigma$  and  $k$  estimated automatically using the technique described in Section 3. Fig. (12) shows the segmentation result of the pendulum using the proposed pressure model of Eq. (21). The old pressure model tends to hover inside the object because of the un-modeled background force, which causes this unbalance at the object boundaries. The performance of the new pressure model is due to modeling the background using a mixture of two Gaussians.

Fig. (13) shows the PDFs of a black and white checkerboard as a target and a light gray and dark gray checkerboard as a background. Fig. (14) shows the result of segmenting the target checkerboard, using the snake of Kass et al. <sup>7</sup>. The segmentation result using the original pressure snakes of Ivins and Porrill <sup>5</sup> is shown in Fig. (15). Fig. (16) shows the segmentation result using the proposed pressure model, with the PDFs estimated as mixtures of Gaussians by the EM algorithm.

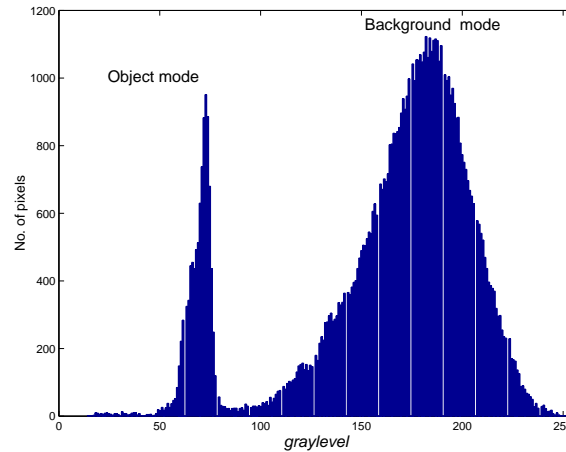


Fig. 6. Histogram of Gray Level Values of Fig. (5)

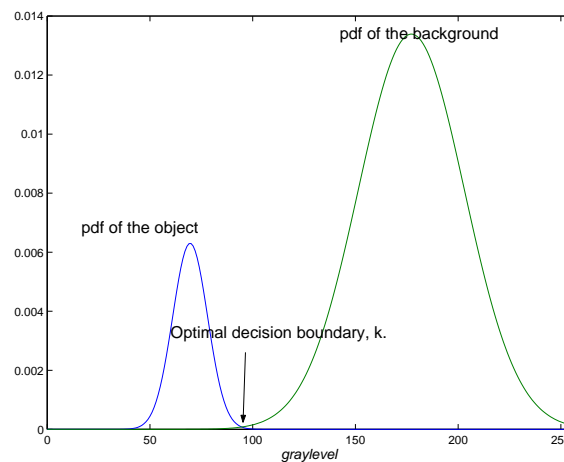


Fig. 7. Estimated PDFs and the optimal decision boundary of Fig. (5), using the approach of Section 3

The Kass et al. <sup>7</sup> fails even with the presence of strong gradient field, because of the complexity of the object and background. The reason why the old pressure snakes fails, however, is due to the un-modeled background color and the simplicity of the object color model. It is worth mentioning here that other techniques might be able to segment the checkerboard (e.g. double thresholding.) However, the comparison here is between the performance of different classes of snakes. Also, estimating the PDFs using Parzen Windows do not affect the segmentation result because of the simplicity of the two PDFs. The Parzen Window technique is helpful when the PDFs cannot be easily estimated using the EM, as will be shown in the next

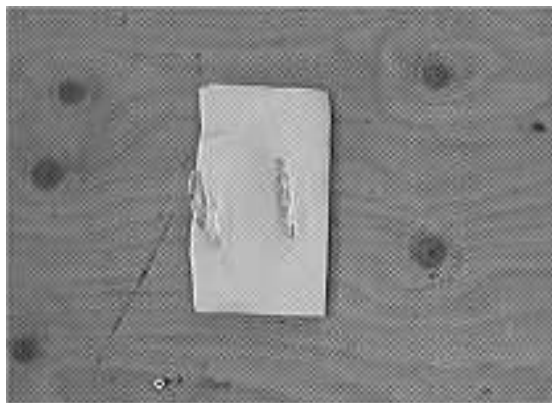


Fig. 8. Complex Colored Background

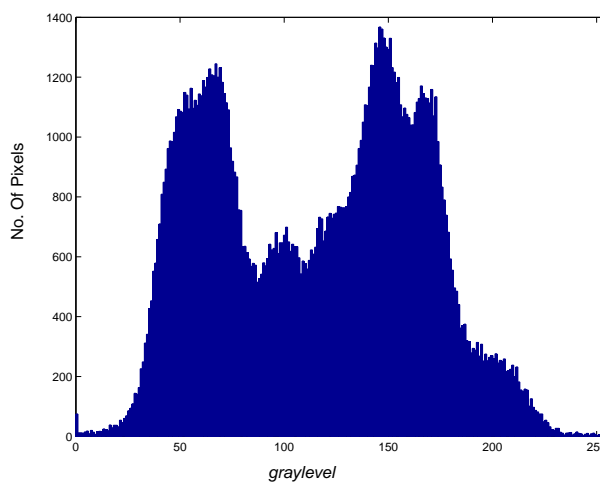


Fig. 9. Histogram of Fig. (8)

experiment.

Fig. (17) presents a real-life image and the segmentation result for the clothing part of a person. The snake is driven using PDFs estimates using Parzen Windows. It is clear that the PDFs of the clothing and the background overlap (because the clothing spans the entire gray scale.) Fig. 18 shows the results of applying the snake to a sequence of images with less number of points to increase the tracking speed.

## 6. Conclusions

In this paper, we presented a new approach to statistical active deformable models. The new approach is based on pattern recognition theory. Several developments

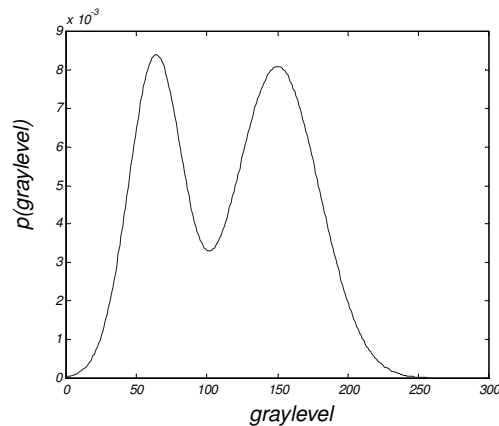


Fig. 10. Estimated PDF of the Background of Fig. (8)

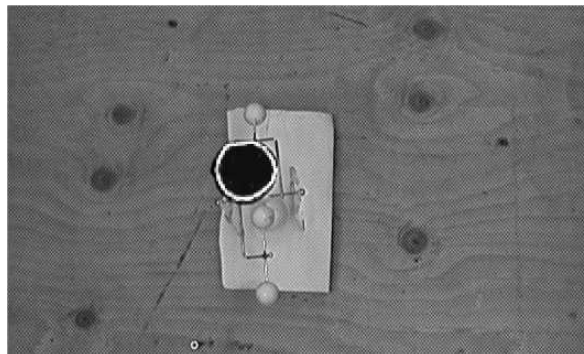


Fig. 11. Tracking Result Using the Pressure Model of Eq. (7), with  $\mu$ ,  $\sigma$  and  $k$  estimated using the algorithm in Section 3.

have been accomplished.

We discussed the advantages of pressure snakes compared to the original snake formulation of Kass et al. <sup>7</sup>. A statistically optimal method for automatically estimating the parameters of pressure snakes was presented. Automatic and accurate estimation of the snake parameters is crucial to obtaining good segmentation results.

The original pressure snake formulation was limited to segmenting simple colored objects. To overcome this drawback, a new generic pressure model was presented. The model is based on the probability density functions of the object and background. The new model has three main advantages. First, the model does not limit the color complexity of the object or the background. The second advantage is that the model accounts for the color complexity of both object and background.

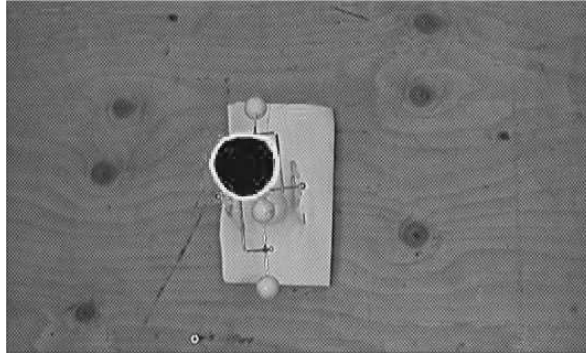


Fig. 12. Tracking Result Using The Generic Pressure Model of Eq. (21), with the density functions estimated using the EM algorithm

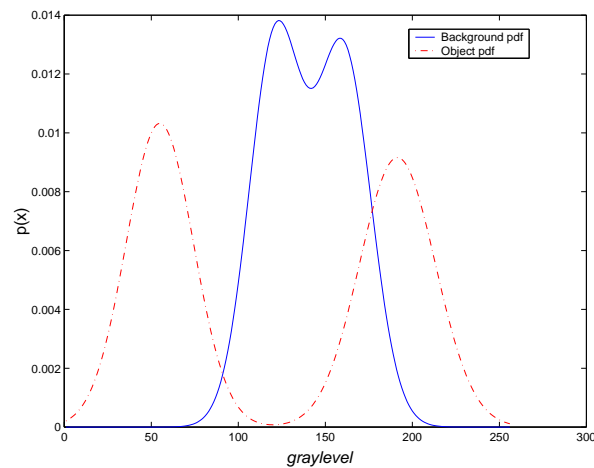


Fig. 13. Estimated PDFs using the EM algorithm of The Object and Background of Fig. (16)

Finally, the model can be used with any extracted feature vector.

Two well-known methods are employed for estimating the PDFs, namely, mixtures of Gaussians and Parzen Windows. Each of the two methods has its advantages and disadvantages. The mixture of Gaussians method has the advantage of providing a functional description of the PDF. This facilitates computing  $p(\mathbf{x})$  directly from the function, most importantly in the case of continuous feature values. There are three main disadvantages for this method. First, the number of Gaussians has to be estimated accurately in order to obtain an accurate PDF. Second, precise initialization of  $\mu$ s and  $\Sigma$ s is required to obtain a good estimate of the PDF. Finally, if the PDF is complex, obtaining correct PDF becomes harder because it requires a large number of components in the mixture.

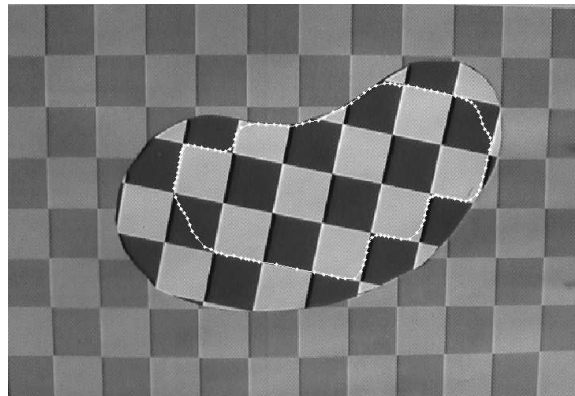


Fig. 14. Checkerboard Segmentation using Kass et al. Snakes

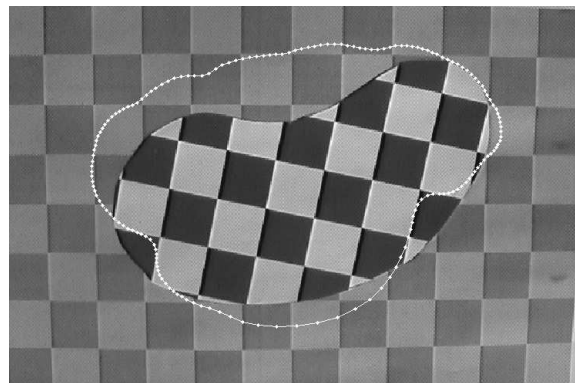


Fig. 15. Checkerboard Segmentation using Ivins and Porrill Snakes

The advantage of the kernel method is that it is easy to obtain an accurate estimate of the PDF, with no parameters to be initialized. The disadvantage is that it works only for discrete feature vector values. In case of continuous feature values, two approaches can be employed. The first is to discretize the feature values before computing  $p(\mathbf{x})$ . The second approach is to compute  $p(\mathbf{x})$  from the original definition of Eq. (25).

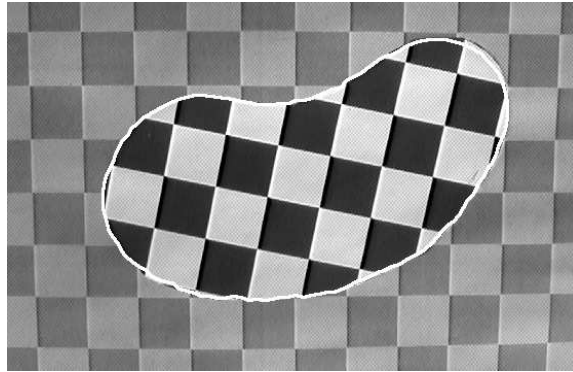


Fig. 16. Object Segmentation using the Generic Pressure Model of Eq. (21) With The PDFs Estimated Using Ehe EM



Fig. 17. Segmentation of Clothing Using the Generic Pressure Model of Eq. (21) and a Snake of 80 Points. The PDFs are Estimated Using The Parzen Window Technique.



Frame No. 1.



Frame No. 5.



Frame No. 30.



Frame No. 55.



Frame No. 80.



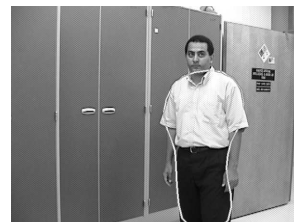
Frame No. 105.



Frame No. 130.



Frame No. 155.



Frame No. 180.



Frame No. 210.



Frame No. 235.



Frame No. 260.

Fig. 18. Tracking Results using the pressure model of Eq. (21) and a 30 Control Point-Snake. The PDFs are estimated using the Parzen Window technique.

### Acknowledgment

The authors would like to thank the anonymous reviewers for their constructive criticism and comments.

### References

1. W. Abd-Almageed, C. Smith and S. Ramadan, "Kernel Snakes: Non-parametric Active Contour Models", *Proc. of the IEEE International Conference on Systems, Man and Cybernetics, Washington D.C., 2003*.
2. W. Abd-Almageed and C. Smith, "Mixture Models for Dynamic Statistical Pressure Snakes", *Proc. of the IEEE International Conference on Pattern Recognition, 2002*, pp. 721-724.
3. S. Ramadan, W. Abd-Almageed and C. Smith, "Eye Tracking Using Active Deformable Models", *Proc. of the IIIrd Indian Conference on Computer Vision, Graphics and Image Processing, 2002*.
4. J. Ivins and J. Porrill, "Active Region Models for Segmenting Medical Images", *Proc. of the IEEE International Conference on Image Processing, 1994*, pp. 227-231
5. J. Ivins and J. Porrill, "Statistical Snakes: Active Region Models", *Fifth British Machine Vision Conference (BMVC), 1994*, vol. 2, pp. 377-386
6. Song Chun Zhu and A. Yuille, "Region Competition: Unifying Snakes, Region Growing and Bayes/MDL for Multiband Image Segmentation", *IEEE Transactions on Pattern Analysis and Machine Intelligence, 1996*, vol. 18, no. 9, pp. 884-900.
7. M. Kass, A. Witkin and D. Terzopoulos, "Snakes: Active Contour Models", *International journal on Computer Vision, 1997*, pp. 321-331.
8. L. Cohen and D. Note, "On Active Contour Models and Balloons", *CVGIP: Image Understanding, 1991*, vol. 53, pp. 211-218.
9. R. Ronfard, "Region-based Strategies for Active Contour Models", *International Journal on Computer Vision, 1994*, vol. 13, p. 229
10. A. P. Dempster, N. M. Laird and D. B. Rubin, "Maximum Likelihood from Incomplete Data via the EM Algorithm", *Journal of Royal Statistical Society* **B39**, (1977), p. 1
11. Rev. T. Bayes, "An Essay toward Solving a Problem in the Doctrine of Chances", *Philosophical Transactions of the Royal Society of London* **Vol. 53**, (1763), p. 370
12. E. Forgy, "Cluster Analysis of Multivariate Data: Efficiency versus Interpretability of Classifications" *Biometry* **Vol. 21**, (1965) p. 768
13. E. M. Aitnouri, S. Wang, D. Ziou, J. Vaillancourt and L. Gagnon, "An Algorithm for Determination of the Number of Modes for pdf Estimation of Multi-Modal Histograms", *Vision Interface '99, Trois-Rivieres, Canada*, (1999), p. 368
14. E. Parzen, "On the Estimation of a Probability Density Function and the Mode", *Math. Statistics*, **Vol. 33**, (1962), p. 1065

## Bibliography



**Wael Abd-Almageed** received the B.S. from the Department of Electronics Engineering in 1994 and the M.S. from the Department of Control and Computers in 1997, both in Mansoura University, Egypt. He also received a Graduate Diploma in Software Engineering from the Information Technology Institute in Egypt in 1997. He received, with Distinction, the Ph.D. from the University of New Mexico (UNM) in 2003. Wael was awarded the Outstanding Graduate Student award from

the Department of Electrical and Computer Engineering at UNM for his Ph.D. research. His research interests are Computer/Robot Vision, Vision-Based User Interfaces and Medical Imaging.

Wael has occupied several industrial positions including Software Engineer, Control Systems Engineer and Research Engineer in Egypt and Canada. He also served as a Visiting Professor at the Department of Electrical Engineering at New Mexico Institute of Mining and Technology. Currently, he is a Research Scientist with the University of Maryland Institute for Advanced Computer Studies (UMIACS).



**Christopher E. Smith** received the B.S. degree in Mathematical and Computer Sciences from Lake Superior State University (Sault Ste. Marie, MI) in 1984, the M.S. degree in Computer Science and Engineering from the University of Michigan (Ann Arbor, MI) in 1987, and the Ph.D. degree in Computer Science from the University of Minnesota (Minneapolis, MN) in 1996. From 1987 to 1989, he was a software engineer with the Defense Systems Division of the Northrop Corporation working on electronic countermeasures.

From 1989 to 1991 he was a senior software engineer the Cellular Infrastructure Group of Motorola working on cellular switch fault management. He was previously an Assistant Professor of Computer Science and Engineering at the University of Colorado at Denver where he was runner up in the 1997-98 College of Engineering Teacher of the Year competition and is currently an Assistant Professor of Electrical and Computer Engineering at the University of New Mexico. He is a member of IEEE, ACM, and AAAI. He is an Associate Editor of the IEEE Transactions on Systems, Man, and Cybernetics: Part A. He has authored or coauthored over 35 journal and conference papers in his areas of research. His research interests include vision-guided robotics, active deformable models, and virtual collaborative

20 *W. Abd-Almageed and C. E. Smith*

environments.